1 mm-thick sections were obtained with a cryostat (5). The RVLM was defined according to a rat brain atlas (27), and the RVLM tissue was obtained using the micro-punch technique (5).

Measurement of TBARS Levels in the RVLM and Whole Brain

Thiobarbituric acid-reactive substances (TBARS) level was measured as a parameter of oxidative stress in the RVLM and whole brain (3,5). The RVLM and whole brain tissues were homogenized in 1.15% KCl (pH 7.4), 0.4% sodium dodecyl sulfate, and 7.5% acetic acid adjusted to pH 3.5 with NaOH. Thiobarbituric acid (0.3%) was added to the homogenate. The mixture was maintained at 5°C for 60 minutes, followed by heating to 100°C for 60 minutes. After cooling, the mixture was extracted with distilled water and *n*-butanolpyridine (15:1) and centrifuged at 1600*g* for 10 minutes. The absorbance of the organic phase was measured at 532 nm. The amount of TBARS was determined by absorbance with a molecular extinction coefficient of 156 000 and expressed as μmol/g wet wt. All values were expressed as the mean ± SEM, and unpaired Student's *t*-test was performed to compare the atorvastatin-treated and the control groups. p values of less than 0.05 were considered significant.

Results

Effects of Atorvastatin on Blood Pressure, Heart Rate, and Urinary Norepinephrine Excretion

Prior to treatment with atorvastatin, SBP, HR, and urinary norepinephrine excretion were significantly higher in SHRSP than in WKY (194 ± 4 mmHg vs. 139 ± 6 mmHg, 388 ± 11 beats/min vs. 348 ± 22 beats/min, 1.38 ± 0.06 μg vs. 0.91 ± 0.06 μg, $p < .05$; n = 5 for each). After 30 days, SBP and urinary norepinephrine excretion in SHRSP were significantly lower in the atorvastatin-treated group than in the control group (173 ± 9 mmHg vs. 199 ± 6 mmHg, 1.07 ± 0.07 μg vs. 1.41 ± 0.04 μg; $p < .05$, n = 5 for each; see Figure 1). After 30 days in WKY, however, there was no significant difference in SBP and urinary norepinephrine excretion between the atorvastatin-treated group and the control group. HR was not significantly different between the atorvastatin-treated group and the control group in SHRSP and WKY (SHRSP: 384 ± 13 beats/min vs. 372 ± 18 beats/min; WKY: 352 ± 26 beats/min vs. 336 ± 24 beats/min).

Effects of Atorvastatin on TBARS Levels in RVLM and Whole Brain

Prior to treatment with atorvastatin, TBARS levels were significantly higher in the RVLM and whole brain of SHRSP than WKY (RVLM: 0.78 ± 0.06 vs. 0.32 ± 0.06 μmol/g wet wt; whole brain: 0.88 ± 0.06 vs. 0.42 ± 0.08 μmol/g wet wt, $p < .05$; n = 5 for each). After 30 days, TBARS levels of RVLM and whole brain in SHRSP were significantly lower in the atorvastatin-treated group than in the control group (RVLM: 0.55 ± 0.03 μmol/g wet wt vs. 0.75 ± 0.04 μmol/g wet wt; whole brain: 0.63 ± 0.04 μmol/g wet wt vs 0.84 ± 0.07 μmol/g wet wt; $p < .05$, n = 5 for each; see Figure 2). After 30 days in WKY, however, there was no significant difference in TBARS levels of RVLM and whole brain between the atorvastatin-treated group and the control group.

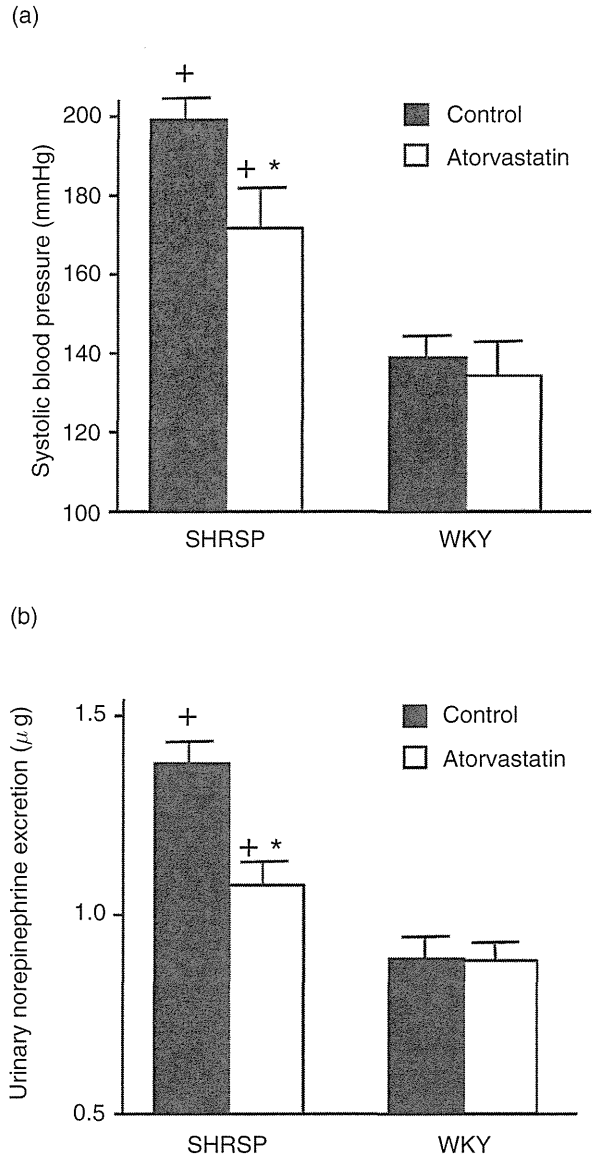

Figure 1. Effects of treatment with atorvastatin for 30 days on (A) systolic blood pressure, and (B) 24-hour urinary norepinephrine excretion in SHRSP and WKY. Male SHRSP and WKY (15 weeks old) were placed on a standard feed diet (control, filled square) or on a standard feed diet supplemented with atorvastatin (50 mg/kg of body weight per day, open square) for 30 days. Systolic blood pressure was assessed with rats in the conscious state using the tail-cuff method. Urinary norepinephrine excretion over 24 hours was measured by high performance liquid chromatography. Data are shown as mean ± SEM (n = 5 per group). *$p < .05$ versus control group in the same strain; †$p < .05$ versus control group in WKY rats after 30 days.

Discussion

The major finding of the present study was that atorvastatin reduced oxidative stress, as measured by a reduction in TBARS levels, in the RVLM of SHRSP, which was significantly increased in SHRSP compared with WKY, and that the antioxidant effect of atorvastatin contributes to the sympatho-inhibitory effect of atorvastatin.

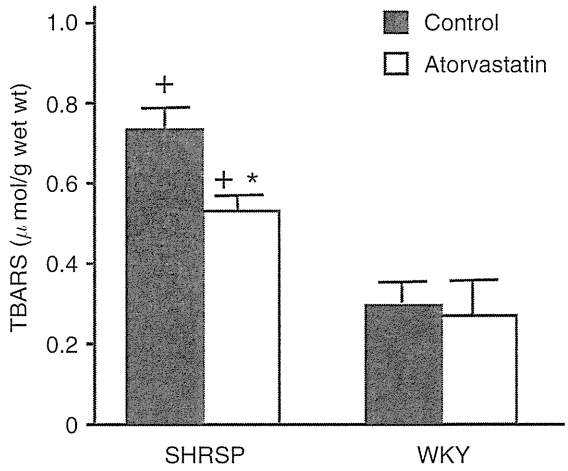

Figure 2. Effects of treatment with atorvastatin for 30 days on TBARS levels in the RVLM of SHRSP and WKY. Male SHRSP and WKY (15 weeks old) were placed on a standard feed diet (control, filled square) or on a standard feed diet supplemented with atorvastatin (50 mg/kg of body weight per day, open square) for 30 days. Data are shown as mean ± SEM (n = 5 per group). $^{*}p < .05$ versus control group in the same strain, $^{\dagger}p < .05$ versus control group in WKY rats after 30 days.

We previously demonstrated that the oral administration of atorvastatin decreased blood pressure in SHRSP (21), and the results of the present study are consistent with those of the previous study. We also suggested that the decrease in blood pressure was due to the sympatho-inhibitory effects of atorvastatin via an increase in NO production in the brain (21). Furthermore, a recent study suggests that oxidative stress in the RVLM increases sympathetic nerve activity (5). Statins have antioxidant effects (10–19,28–29), and alterations in the balance between NO and superoxide are implicated in hypertension (30–31). Statins increase thioredoxin activity by an NO-dependent pathway (32), which might be another mechanism through which improved NO availability promotes endogenous vascular antioxidant defense systems. Statin treatment inhibits the activation of the oxidant enzyme system NAD (P) H oxidase, likely by preventing a membrane translocation of the small G protein rac-1 (15,33), which might contribute to reduced vascular oxidant stress after statin treatment. These studies suggest that statin upregulates NO bioavailability and has antioxidant effects. The RVLM is known as the vasomotor center, and NO and oxidative stress in the RVLM are important factors regulating the sympathetic nerve activity (5,23–26). These results suggest that the oral administration of atorvastatin has antioxidant effects in the RVLM of SHRSP as a pleiotropic effect, and these antioxidant effects induce the upregulation of NO production in the RVLM of SHRSP, as well as sympatho-inhibitory effects. Furthermore, statins enhance endothelial NO bioavailability by both promoting endothelial NO production (14,34–36) and preventing NO inactivation by radicals (15). The decreases in oxidative stress by the oral administration of atorvastatin in the RVLM are thought to induce a sympatho-inhibitory effect because oxidative stress in the RVLM causes sympatho-excitatory effects (5).

Recent clinical and animal studies suggest that statins exert protective effects against nonhemorrhagic stroke (37–39). Moreover, statins improve the outcome of acute ischemic stroke in humans (37). In SHRSP, rosuvastatin attenuates inflammatory processes associated with cerebrovascular disease by increasing the transcription of

eNOS mRNA, preventing endothelial dysfunction, reducing production of ROS, and inhibiting leukocyte-endothelial adhesion (40). Furthermore, statins improve the outcome after myocardial infarction or stroke by LDL cholesterol-independent, eNOS-dependent mechanisms (10,41,42). In this study, the antioxidant effects of atorvastatin were not specific in the RVLM and we confirmed that atorvastatin has antioxidant effects in the whole brain. We demonstrated that sympathetic nerve activity was increased in the SHRSP (5,21) and a previous study reported that the densities of noradrenergic nerve fibers in the epicardium and myocardium are significantly higher in SHRSP than in WKY (37). The sympatho-inhibitory effects of atorvastatin might also contribute to the protective effects against stroke.

We measured TBARS levels as the parameter of oxidative stress in the brain. TBARS levels are widely used as a marker of oxidative stress (3–5). TBARS levels, however, are an indirect marker of oxidative stress. Previously, we directly measured oxidative stress in the brain of SHRSP and WKY using electron spin resonance spectroscopy and confirmed that TBARS levels are comparable to the levels of oxidative stress measured by electron spin resonance spectroscopy in the brain (5). These results suggest that TBARS levels are a valid parameter of oxidative stress in the brain.

In the present study, we used atorvastatin only and did not perform experiments to examine the effect of other statins. It is not known whether the antioxidant effect of atorvastatin in the brain is a specific effect of atorvastatin or a general effect of all statins. Further studies are necessary.

Conclusion

The oral administration of atorvastatin for 30 days reduced blood pressure, urinary norepinephrine excretion, and TBARS levels in the RVLM of SHRSP. These results suggest that the antioxidant effect of atorvastatin in the RVLM might contribute to the sympatho-inhibitory effects in SHRSP through the upregulation of NO bioavailability by the scavenger effect of oxidative stress against NO and the decrease in the sympatho-excitatory effect of oxidative stress.

Acknowledgments

This work was supported by Grants-in-Aid for Scientific Research from the Japan Society for the Promotion of Science (C15590757, C17590745) and, in part, by the Health and Labor Sciences Research Grant for Comprehensive Research in Aging and Health Labor and Welfare of Japan.

References

1. Kerr S, Brosnan J, McIntyre M, Reid JL, Dominiczak AF, Hamilton CA. Superoxide anion production is increased in a model of genetic hypertension. *Hypertension*. 1999;33:1353–1358.
2. Nakazono K, Watanabe N, Matsuno K, Sakai J, Sato T, Inoue M. Does superoxide underlie the pathogenesis of hypertension? *Proc Natl Acad Sci USA*. 1991;88:10045–10048.
3. Ohtsuki T, Matsumoto M, Suzuki K, Taniguchi N, Kamada T. Mitochondrial lipid peroxidation and superoxide dismutase in rat hypertensive target organs. *Am J Physiol*. 1995;268:H1418–H1421.
4. Kimoto-Kinoshita S, Nishida S, Tomura TT. Age-related change of antioxidant capacities in the cerebral cortex and hippocampus of stroke-prone spontaneously hypertensive rats. *Neurosci Lett*. 1999;273:41–44.

5. Kishi T, Hirooka Y, Kimura Y, Ito K, Shimokawa H, Takeshita A. Increased reactive oxygen species in rostral ventrolateral medulla contribute to neural mechanisms of hypertension in stroke-prone spontaneously hypertensive rats. *Circulation*. 2004;109:2357–2362.
6. Randomized trial of cholesterol lowering in 4444 patients with coronary heart disease: The Scandinavian Simvastatin Survival study (4S). *Lancet*. 1994;344:1383–1389.
7. Prevention of cardiovascular events and death with pravastatin in patients with coronary heart disease and a broad range of initial cholesterol levels. The Long-Term Intervention with Pravastatin in Ischemic Disease (LIPID) Study Group. *N Engl J Med*. 1998;339:1349–1357.
8. Sever PS, Dahlof B, Poulter NR, Wedel H, Beevers G, Caulfield M, Nieminen M, O'Brien E, Ostergren J. Prevention of coronary and stroke events with atorvastatin in hypertensive patients who have average or lower-than-average cholesterol concentrations, in the Anglo-Scandinavian Cardiac Outcomes Trial-Lipid Lowering Arm (ASCOT-LLA): A multicentre randomized controlled trials. *Lancet*. 2003;361:1149–1158.
9. Glorioso N, Troffa C, Filigheddu F, Dettori F, Soro A, Parpaglia PP, Collatina S, Pahor M. Effect of the HMG-CoA reductase inhibitors on blood pressure in patients with essential hypertension and primary hypercholesterolemia. *Hypertension*. 1999;34:1281–1286.
10. Endres M, Laufs U, Huang Z, Nakamura T, Huang P, Moskowitz MA, Liao JK. Stroke protection by 3-hydroxy-3-methylglutaryl (HMG)-CoA reductase inhibitors mediated by endothelial nitric oxide synthase. *Proc Natl Acad Sci USA*. 1998;95:8880–8885.
11. Wassmann S, Laufs U, Baumer AT, Muller K, Ahlbory K, Linz W, Itter G, Rosen R, Bohm M, Nickenig G. HMG-CoA reductase inhibitors improve endothelial dysfunction in normocholesterolemic hypertension via reduced production of reactive oxygen species. *Hypertension*. 2001;37:1450–1457.
12. O'Driscoll G, Green D, Taylor RR. Simvastatin, an HMG-coenzyme A reductase inhibitor, improves endothelial function within one month. *Circulation*. 1997;95:1126–1131.
13. Mital S, Zhang X, Zhao G, Bernstein RD, Smith CJ, Fulton DL, Sessa WC, Liao JK, Hintze TH. Simvastatin upregulates coronary endothelial nitric oxide production conscious dogs. *Am J Physiol*. 2000;279:H2649–H2657.
14. Laufs U, LaFata V, Plutzky J, Liao JK. Upregulation of endothelial nitric oxide synthase by HMG-CoA reductase inhibitors. *Circulation*. 1998;97:1129–1135.
15. Wassmann S, Laufs U, Muller K, Konkol C, Ahlbory K, Baumer AT, Linz W, Bohm M, Nickenig G. Cellular antioxidant effects of atorvastatin in vitro and in vivo. *Arterioscler Thromb Vasc Biol*. 2002;22:300–305.
16. Laufs U, Liao JK. Isoprenoid metabolism and the pleiotropic effects of statins. *Curr Atheroscler Rep*. 2003;5:372–378.
17. Palinski W. New evidence for beneficial effects of statins unrelated to lipid lowering. *Atheroscler Thromb Vasc Biol*. 2001;21:3–5.
18. Llevadot J, Murasawa S, Kureishi Y, Uchida S, Masuda H, Kawamoto A, Walsh K, Isner JM, Asahara T. HMG-CoA reductase inhibitor mobilizes bone marrow-derived endothelial progenitor cells. *J Clin Invest*. 2001;108:399–405.
19. Vasa M, Fichtlscherer S, Adler K, Aicher A, Martin H, Zeiher AM, Dimmeler S. Increase in circulating endothelial progenitor cells by statin therapy in patients with stable coronary artery disease. *Circulation*. 2001;103:2885–2890.
20. Landmesser U, Bahlmann F, Mueller BS, Spiekermann S, Kirchhoff N, Schulz S, Manes C, Fischer D, De Groot K, Fliser D, Fauler G, Marz W, Drexler H. Simvastatin versus ezetimibe: Pleiotropic and lipid-lowering effects on endothelial function in humans. *Circulation*. 2005;111:2356–2363.
21. Kishi T, Hirooka Y, Mukai Y, Shimokawa H, Takeshita A. Atorvastatin causes depressor and sympatho-inhibitory effects with upregulation of nitric oxide synthases in stroke-prone spontaneously hypertensive rats. *J Hypertens*. 2003;21:379–386.
22. Hamilton CA, Brosnan MJ, Mclntyre M, Graham D, Dominiczak AF. Superoxide excess in hypertension and aging. *Hypertension*. 2001;37:529–534.

23. Sakai K, Hirooka Y, Matsuo I, Eshima K, Shigematsu H, Shimokawa H, Takeshita A. Overexpression of eNOS in NTS causes hypotension and bradycardia in vivo. *Hypertension.* 2000;36:1023–1028.
24. Hirooka Y, Sakai K, Kishi T, Takeshita A. Adenovirus-mediated gene transfer into the NTS in conscious rats: a new approach to examining the central control of cardiovascular regulation. *Ann NY Acad Sci.* 2001;940:197–205.
25. Kishi T, Hirooka Y, Sakai K, Shigematsu H, Shimokawa H, Takeshita A. Overexpression of eNOS in the RVLM causes hypotension and bradycardia via GABA release. *Hypertension.* 2001;38:896–901.
26. Kishi T, Hirooka Y, Ito K, Sakai K, Shimokawa H, Takeshita A. Cardiovascular effects of overexpression of endothelial nitric oxide synthase in the rostral ventrolateral medulla in stroke-prone spontaneously hypertensive rats. *Hypertension.* 2002;39:264–268.
27. Paxinos G, Watson C. *The Rat Brain in Stereotaxic Coordinates*. New York: Academic Press; 1998.
28. Rikitake Y, Kawashima S, Takeshita S, Yamashita T, Azumi H, Yasuhara M, Nishi H, Inoue N, Yokoyama M. Anti-oxidative properties of fluvastatin, an HMG-CoA reductase inhibitor, contribute to prevention of atherosclerosis in cholesterol-fed rabbits. *Atherosclerosis.* 2001;154:87–96.
29. Thakur NK, Hayashi T, Sumi D, Kano H, Tsunekawa T, Iguchi A. HMG-CoA reductase inhibitor stabilizes rabbit atheroma by increasing basal NO and decreasing superoxide. *Am J Physiol.* 2001;281:H75–H83.
30. Delanty N, Vaughan CJ. Vascular effects of statins in stroke. *Stroke.* 1997;28:2315–2320.
31. The Long-Term Intervention with Pravastatin in Ischemic Disease (LIPID) Study Group. Prevention of cardiovascular events and death with pravastatin in patients with coronary heart disease and a broad range or initial cholesterol levels. *N Engl J Med.* 1998;339:1349–1357.
32. Haendeler J, Hoffmann J, Zeiher AM, Dimmler S. Antioxidant effects of statins via S-nitrosylation and activation of thioredoxin in endothelial cells: A novel vasculoprotective function of statins. *Circulation.* 2004;110:856–861.
33. Maack C, Kartes T, Kilter H, Schafers HJ, Nickenig G, Bohm M, Laufs U. Oxygen free radical release in human failing myocardium is associated with increased activity of rac1-GTPase and represents a target for statin treatment. *Circulation.* 2003;108:1567–1574.
34. Kureishi Y, Luo Z, Shiojima I, Bialik A, Fulton D, Lefer DJ, Sessa WC, Walsh K. The HMG-CoA reductase inhibitor simvastatin activates the protein kinase Akt and promotes angiogenesis in normocholesterolemic animals. *Nat Med.* 2000;6:1004–1010.
35. Feron O, Dessy C, Desager JP, Balligand JL. Hydroxy-methylglutaryl-coenzyme A reductase inhibition promotes endothelial nitric oxide synthase activation through a decrease in caveolin abundance. *Circulation.* 2001;103:113–118.
36. Kalinowski L, Dobrucki LW, Brovkovych V, Malinski T. Increase nitric oxide bioavailability in endothelial cells contributes to the pleiotropic effect of cerivastatin. *Circulation.* 2002;105:933–938.
37. Kondo M, Terada M, Fujiwara T, Arita N, Yano A, Tabei R. Noradrenergic hyperinnervation in the heart of stroke-prone spontaneously hypertensive rats. *Clin Exp Pharmacol Physiol Suppl.* 1995;22:S75–S76.
38. Cilla DD, Whitefield LR, Gibson DM, Sedman AJ, Posvar EL. Multiple-dose pharmacodynamics, and safety of atorvastatin, an inhibitor of HMG-CoA reductase, in healthy subjects. *Clin Pharmacol Ther.* 1996;60:687–695.
39. Moonis M, Kane K, Schwiderski U, Sandage BW, Fisher M. HMG-CoA reductase inhibitors improve acute ischemic stroke outcome. *Stroke.* 2005;36:1298–1300.
40. Sironi L, Gianazza E, Gelosa P, Guerrini U, Nobili E, Gianella A, Cremonesi B, Paoletti R, Tremoli E. Rosuvastatin, but not simvastatin, provides end-organ protection in stroke-prone rats by anti-inflammatory effects. *Arterioscler Thromb Vasc Biol.* 2005;25:598–603.

41. Di Napoli P, Antonio Taccardi A, Grilli A, Spina R, Felaco M, Barsotti A, De Caterina R. Simvastatin reduces reperfusion injury by modulating nitric oxide synthase expression: An ex vivo study in isolated working rat hearts. *Cardiovasc Res*. 2001;51:283–293.
42. Landmesser U, Engberding N, Bahlmann F, Schaefer A, Wiencke A, Heineke A, Spiekermann S, Hilfiker-Kleiner D, Templin C, Kotlarz D, Mueller M, Hornig B, Haller H, Drexler H. Statin-induced improvement of endothelial progenitor cell mobilization, myocardial neovascularization, LV function, and survival after experimental myocardial infarction requires endothelial nitric oxide synthase. *Circulation*. 2004;110:1933–1939.

Available online at www.sciencedirect.com
ScienceDirect
Biochemical and Biophysical Research Communications 367 (2008) 474–480
BBRC
www.elsevier.com/locate/ybbrc

Involvement of Mst1 in tumor necrosis factor-α-induced apoptosis of endothelial cells

Hideki Ohtsubo [a], Toshihiro Ichiki [a,*], Ikuyo Imayama [a], Hiroki Ono [a], Kae Fukuyama [a], Yasuko Hashiguchi [a], Junichi Sadoshima [b], Kenji Sunagawa [a]

[a] *Department of Cardiovascular Medicine, Kyushu University Graduate School of Medical Sciences, 3-1-1 Maidashi, Higashi-ku, 812-8582 Fukuoka, Japan*
[b] *Cardiovascular Research Institute, University of Medicine and Dentistry of New Jersey, USA*

Received 25 December 2007
Available online 7 January 2008

Abstract

Mammalian sterile 20-kinase 1 (Mst1), a member of the sterile-20 family protein kinase, plays an important role in the induction of apoptosis. However, little is know about the physiological activator of Mst1 and the role of Mst1 in endothelial cells (ECs). We examined whether Mst1 is involved in the tumor necrosis factor (TNF)-α-induced apoptosis of ECs. Western blot analysis revealed that TNF-α induced activation of caspase 3 and Mst1 in a time- and dose-dependent manner. TNF-α-induced Mst1 activation is almost completely prevented by pretreatment with Z-DEVD-FMK, a caspase 3 inhibitor. Nuclear staining with Hoechst 33258 and fluorescence-activated cell sorting of propidium iodide-stained cells showed that TNF-α induced apoptosis of EC. Diphenyleneiodonium, an inhibitor of NADPH oxidase, and *N*-acetylcysteine, a potent antioxidant, also inhibited TNF-α-induced activation of Mst1 and caspase 3, as well as apoptosis. Knockdown of Mst1 expression by short interfering RNA attenuated TNF-α-induced apoptosis but not cleavage of caspase 3. These results suggest that Mst1 plays an important role in the induction of TNF-α-induced apoptosis of EC. However, positive feedback mechanism between Mst1 and caspase 3, which was shown in the previous studies, was not observed. Inhibition of Mst1 function may be beneficial for maintaining the endothelial integrity and inhibition of atherogenesis.

Keywords: TNF-α; Apoptosis; Mst1; Caspase 3; Reactive oxygen species

Endothelial dysfunction induced by inflammatory mediators plays a pivotal role in the initiation and progression of atherosclerosis [1,2]. In more advanced atherosclerotic plaques, inflammatory cells such as T lymphocytes and monocytes/macrophages are observed [3–5]. Tumor necrosis factor-α (TNF-α), a potent inflammatory cytokine, is produced from these inflammatory cells, endothelial cells (ECs), and vascular smooth muscle cells (VSMCs) [6]. TNF-α up-regulates expression of cellular adhesion molecules on EC surfaces as well as induces apoptosis of ECs [7]. TNF-α activates matrix metalloproteinases (MMP) in VSMCs [8,9]. Degradation of extracellular matrix by MMP weakens the fibrous cap of atherosclerotic plaques and makes the lesion unstable [10,11]. Plaque rupture appears to be a complication of these insidious processes of chronic inflammation of blood vessels [12–14], and is believed to be responsible for acute coronary syndrome.

An increase in EC and SMC apoptosis is a common feature of unstable plaque, suggesting that apoptosis might contribute to plaque erosion and development of acute coronary syndrome [15,16]. Expression of Bax, a pro-apoptotic protein, is increased in EC overlying atherosclerotic lesions while expression of anti-apoptotic factor, Bcl-2, is decreased [17,18]. Knowledge of the key regulatory molecules of EC apoptosis may offer novel therapeutic targets in both prevention and treatment of atherosclerosis and plaque rupture.

Mammalian sterile 20-like kinase 1 (Mst1) is a ubiquitously expressed serine/threonine kinase, and belongs to a mammalian sterile 20-like kinase (Ste20) family [19]. Mst1 is cleaved by caspase 3 and this cleavage increases

* Corresponding author. Fax +81 92 642 5374.
E-mail address: ichiki@cardiol.med.kyushu-u.ac.jp (T. Ichiki).

0006-291X/$ - see front matter © 2007 Elsevier Inc. All rights reserved.
doi:10.1016/j.bbrc.2007.12.173

kinase activity of Mst1 by removal of the regulatory C-terminal region, which in turn activates caspase 3 [20]. Therefore, cleavage of Mst1 is considered as a surrogate marker of activation. Thus, Mst1 and caspase 3 constitute a positive feedback loop that amplifies apoptotic responses. Although it has been reported that non-physiological stimuli such as chelerythrine [21] and staurosporine [22] activate Mst1 and induce apoptosis, physiological activators of Mst1 have never been reported except for Fas/Fas ligand pathway [23]. In addition, the role of Mst1 in the apoptosis of EC has not been examined so far.

We examined whether Mst1 is involved in TNF-α-induced apoptosis of EC.

Material and methods

Materials. Dulbecco's modified Eagle's medium (DMEM) was purchased from GIBCO BRL. Fetal bovine serum (FBS) was from JRH Biosciences Inc. Bovine serum albumin (BSA) was purchased from Sigma Chemical Co. Diphenyleneiodonium (DPI) was purchased from Research Biochemicals Intl. and *N*-acetylcysteine (NAC) was purchased from Sigma–Aldrich Co. Horseradish-peroxidase conjugated secondary antibodies (anti-rabbit or anti-mouse IgG) were purchased from VECTOR Laboratories Inc. Other antibodies used in the experiments were obtained from Cell Signaling Technology. Z-DEVD-FMK was purchased from R&D Systems, Inc. Other chemical reagents were purchased from Wako Pure chemicals unless specifically mentioned.

Cell culture. All procedures and care of the animals were approved by the Committee on Ethics of Animal Experiments, Kyushu University. ECs were isolated from the thoracic aorta of bovine and grown in a humidified atmosphere of 95% air/5% CO_2 at 37 °C in DMEM with 10% FBS. Cells between passage 5 and 14 were used for the experiments.

Adenovirus vector expressing Mst1 and empty adenovirus vector. A recombinant adenovirus vectors expressing Mst1 (AdMst1) was reported previously [21]. Confluent ECs were washed two times with phosphate-buffered saline (PBS) and incubated with AdMst1 or an empty adenovirus vector (Ad1W) under gentle agitation for 2 h at room temperature. Then the cells were washed 3 times with PBS, cultured in DMEM with 10% FBS for 2 days and used for the experiments. Multiplicity of infection (m.o.i) indicates the number of virus per cell added to a culture dish.

Detection of apoptosis. Cells infected with AdMst1 and Ad1W, were stimulated with TNF-α and isolated through trypsinization. The isolated cells and cells in the medium were collected by centrifugation and stained with Hoechst 33258. The number of apoptotic cells (cell shrinkage, chromatin condensation and nuclear fragmentation) was counted from 100 cells under fluorescence microscopy. Counting was performed in five independent fields. Fluorescence-activated cell sorting (FACS; EPICS ALTRA MultiCOMP, BECKMAN COULTER) analysis of propidium iodide-stained cells was also performed to detect apoptosis. FACS analysis counted the number of apoptotic cells (hypodiploid cells) per 10,000 cells as described previously [24].

Western blot analysis. ECs were lysed in a sample buffer (5 mmol/L EDTA, 10 mmol/L Tris–HCl, pH 7.6, 1% Triton X-100, 50 mmol/L NaCl, 30 mmol/L sodium phosphate, 50 mmol/L NaF, 1% aprotinin, 0.5%

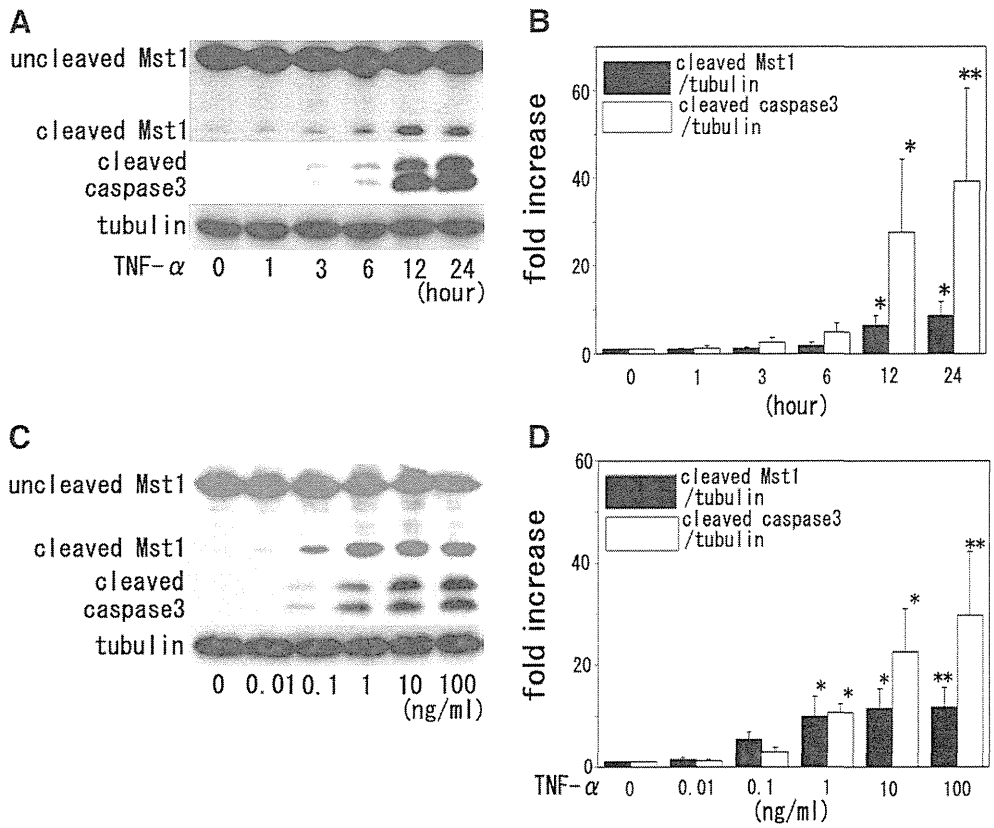

Fig. 1. Activation of Mst1 and caspase 3 by TNF-α. (A) BECs were stimulated with TNF-α (10 ng/mL) for various periods as indicated in the figure, and cleavage of Mst1 and caspase 3 was detected by Western blot analysis. (B) The ratio of cleaved Mst1 or caspase 3 to α-tubulin is shown as a relative fold increase compared with that in control cells. (C) BECs were stimulated with TNF-α at various concentrations for 12 h. Cleavage of Mst1 and caspase 3 were detected by Western blot analysis. (D) The ratio of cleaved Mst1 or caspase 3 to α-tubulin is shown as a relative fold increase compared with that in control cells. The same results were obtained in other independent experiments ($n = 4$). The values are expressed as means ± SEM. $^{*}p < 0.05$ versus control, $^{**}p < 0.01$ versus control.

pepstatin A, 2 mmol/L phenylmethylsulfonyl fluoride and 5 mmol/L leupeptin). After electrophoresis on SDS–polyacrylamide gel, which is followed by transfer to polyvinylidene fluoride membrane, Western blot analyses of Mst1 and cleaved caspase 3 were performed as described previously [25]. Densitometric analysis of cleaved caspase 3 took account of two cleaved bands (19 and 17 KDa).

Short interfering RNA. The annealed form of siRNA of Mst1 was constructed from a 21 base pair (bp) of Mst1 (NCBI nucleotide accession number XM_615482) by Samchully Pharm. Co. The optimal Mst1 sequence was CAA GCG AAA UAC AGU GAU ATT. This region corresponds to bovine Mst1 gene located approximately 747 bp downstream from the transcription start site. For the control siRNA, a scrambled sequence (GCA UAG AGG ACA ACU AAA UTT) that does not contain any significant homology to bovine Mst1 sequence was used. Introduction of siRNA and scrambled RNA (scRNA) for Mst1 to ECs was performed by lipofection (Lipofectoamine 2000, Invitrogen Co.) according to manufacturer's instruction.

Statistical analysis. Statistical analysis was performed with one-way ANOVA and Fisher's test if appropriate. $p < 0.05$ was considered to be statistically significant. Data are shown as means ± SEM.

Results

TNF-α induced activation of Mst1 and caspase 3 in bovine aortic EC

Cleavage of Mst1 or caspase 3 is known to increase their activities [23], and can be used as a surrogate marker of activation. Therefore, we used Western blot analysis that detects cleavage of Mst1 or caspase 3. Western blot analysis revealed that TNF-α induced cleavage of Mst1 and caspase 3 in a time- and dose-dependent manner (Fig. 1). The time course of the cleavage of Mst1 and caspase 3 is very similar. These data suggest that Mst1 and caspase 3 are activated by TNF-α.

Caspase 3 plays an important role in TNF-α-induced cleavage of Mst1

Preincubation with Z-DEVD-FMK (100 μmol/L), a specific inhibitor of caspase 3, for 30 min almost completely inhibited cleavage of Mst1 induced by TNF-α (Fig. 2A and B), suggesting that Mst1 is activated in the downstream from caspase 3. Z-DEVD-FMK did not prevent cleavage of caspase 3 (Fig. 2C and D).

TNF-α and AdMst1 induced apoptosis of ECs

Staining with Hoechst 33258 (Fig. 3A–E) and FACS analysis (Fig. 3F) showed that TNF-α increased the number of apoptotic cells, characterized by chromatin condensation and nuclear fragmentation. Overexpression of Mst1 also increased the number of apoptotic ECs as previously described [24].

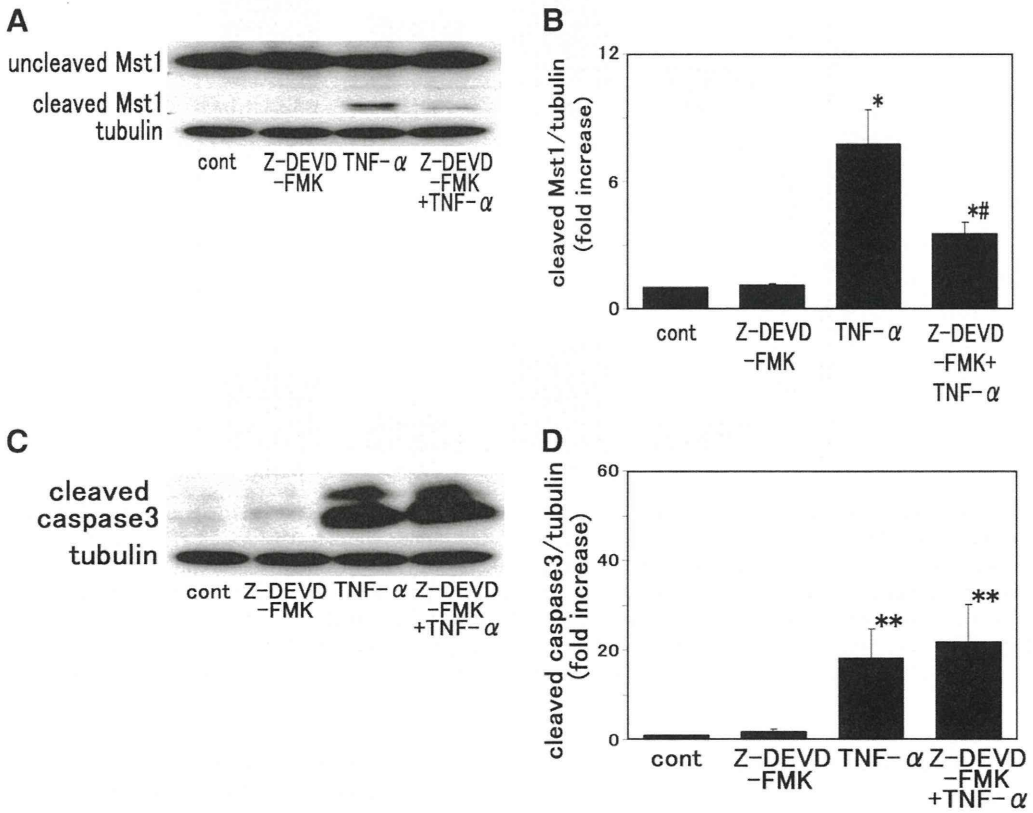

Fig. 2. TNF-α-induced activation of Mst1 was inhibited by pretreatment with Z-DEVD-FMK. BECs were preincubated with Z-DEVD-FMK (100 μmol/L), a specific inhibitor of caspase 3, for 30 min, and then stimulated with TNF-α (10 ng/mL) for 12 h. (A) Cleavage of Mst1 was detected by Western blot analysis. (B) The ratio of cleaved Mst1 to α-tubulin is shown as a relative fold increase compared with that in control cells. The same results were obtained in other independent experiments ($n = 4$). (C,D) Effect of Z-DEVD-FMK on TNF-α-induced caspase 3 cleavage was also examined and analyzed by Western blot analysis. ($n = 4$) The values are expressed as means ± SEM. $^{*}p < 0.05$, $^{**}p < 0.01$ versus control, $^{\#}p < 0.05$ versus TNF-α.

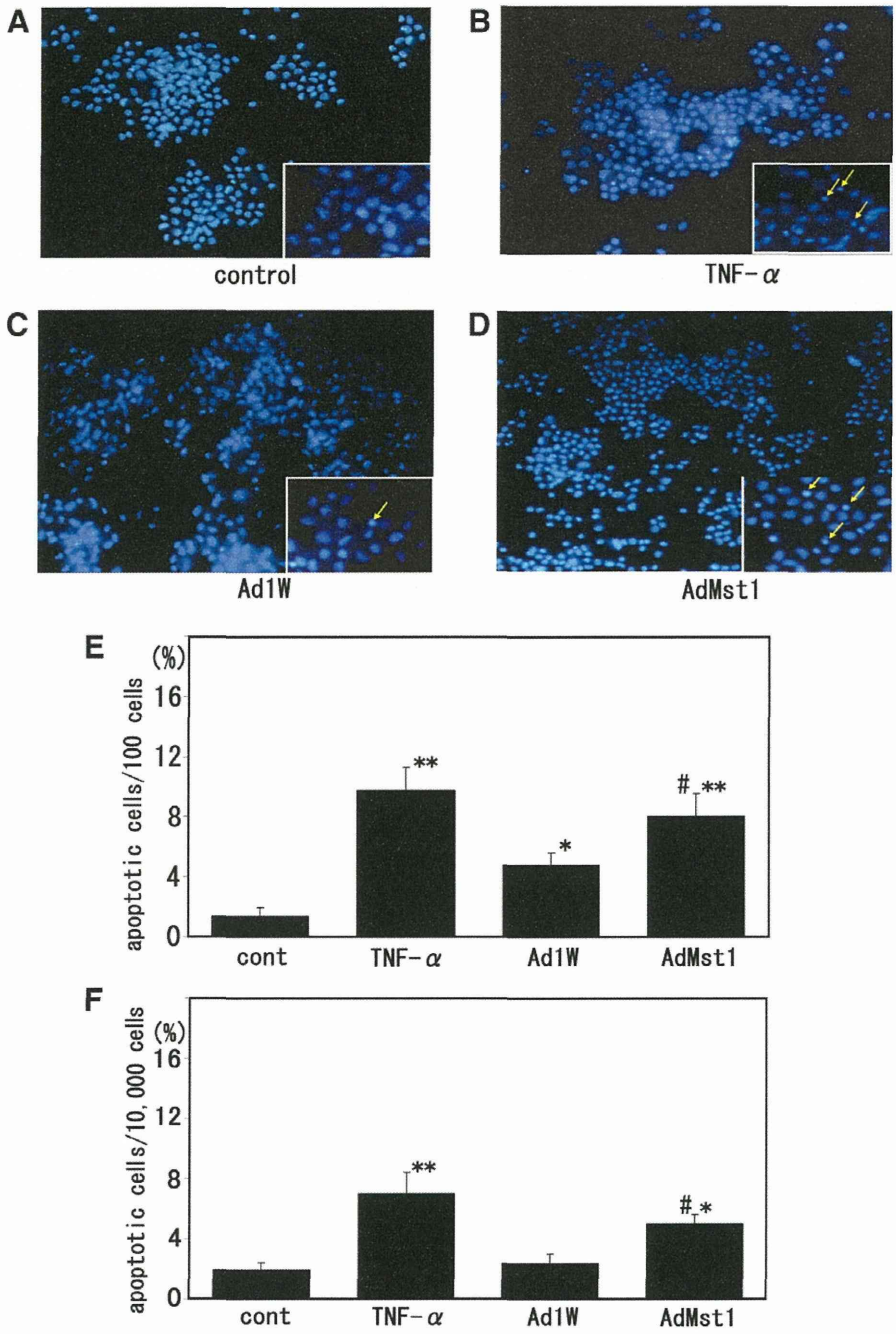

Fig. 3. TNF-α and overexpression of Mst1 induced apoptosis of ECs. (A) Unstimulated BECs, (B) TNF-α (10 ng/mL, 24 h)-stimulated BECs, (C) Ad1W-infected BECs (10MOI, 48 h), and (D) AdMst1-infected BECs (10MOI, 48 h) were stained with Hoechst 33258. (E) The number of cells with chromatin condensation or fragmentation was counted per 100 cells under fluorescence microscopy. Representative microphotographs are shown. Arrows indicate chromatin condensation or fragmentation. Counting was performed in five independent fields. The average number of apoptotic cells per 100 cells is shown as a bar graph ($n = 4$). (F) Unstimulated BECs, TNF-α (10 ng/mL, 24 h)-stimulated BECs, Ad1W-infected BECs (10MOI, 48 h), and AdMst1-infected BECs (10MOI, 48 h) were stained with PI. Apoptotic cells (hypodiploid) per 10,000 BECs were counted by flow cytometry. Proportion of apoptotic cells were shown as a bar graph ($n = 4$). $^{*}p < 0.05$ versus control, $^{**}p < 0.01$ versus control, $^{\#}p < 0.05$ versus Ad1W.

TNF-α induces activation of Mst1 and caspase 3 via reactive oxygen species

It has been reported that reactive oxygen species (ROS) are involved in cell death signaling [26]. To investigate the role of ROS in TNF-α-induced Mst1 and caspase 3 activation, we examined the effect of DPI and NAC. Both DPI and NAC inhibited the TNF-α-induced activation of Mst1. DPI and NAC partially inhibited the TNF-α-induced caspase 3 activation. FACS analysis showed that both DPI and NAC significantly inhibited the TNF-α-induced apoptosis. These data suggest that the TNF-α-induced apoptosis is, at least in part, dependent on ROS-mediated-activation of Mst1 and caspase 3 (Supplementary Fig. 1).

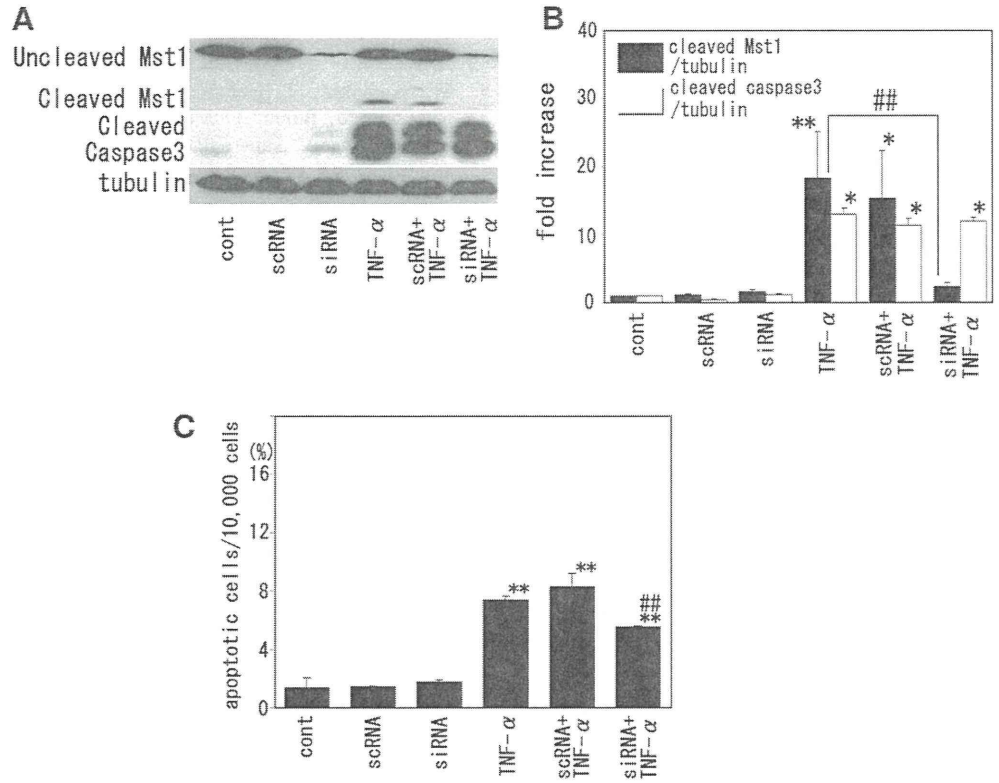

Fig. 4. siRNA for Mst1 attenuated TNF-α-induced apoptosis. BECs were stimulated with TNF-α (10 g/ml, 24 h) after introduction of siRNA or scRNA for Mst1 by lipofection method. (A) Cleavage of Mst1 and caspase 3 was detected by Western blot analysis. (B) The ratio of cleaved Mst1 or caspase 3 to α-tubulin is shown as a relative fold increase compared with that in control cells. BECs were stimulated with TNF-α for 12 h after an introduction of siRNA or scRNA for Mst1. (C) Apoptotic cells per 10,000 BECs stained with PI were counted by flow cytometry. Proportion of apoptotic cells was shown as a bar graph ($n = 4$). The values are expressed as means ± SEM. $^{*}p < 0.05$, $^{**}p < 0.01$ versus control, $^{\#\#}p < 0.01$ versus TNF-α.

Knockdown of Mst1 by siRNA attenuated TNF-α-induced apoptosis

To confirm the role of Mst1 in TNF-α-induced EC apoptosis, endogenous Mst1 was knocked down by siRNA. scRNA was used as a control. Introduction of siRNA for Mst1 significantly decreased expression of uncleaved Mst1 in unstimulated cells (Fig. 4A), whereas scRNA did not. TNF-α-induced cleavage of Mst1 was hardly detected in siRNA-treated ECs (Fig. 4A and B), whereas cleavage of caspase 3 was not affected. Introduction of siRNA for Mst1 attenuated TNF-α-induced apoptosis of EC (Fig. 4C).

Discussion

In the present study, we demonstrated that Mst1, at least in part, mediates TNF-α-induced apoptosis of ECs. To the best of our knowledge, this is the first report showing the activation of Mst1 by TNF-α. Although previous studies showed that Mst1 and caspase 3 form a positive feedback loop and accelerate apoptotic process, this is not the case as to TNF-α-induced apoptosis of ECs because downregulation of Mst1 by siRNA did not affect TNF-α-induced caspase 3 activation.

ROS have been reported to be involved in the process of cell death signaling [26,27]. Kamata et al. [28] reported that ROS promotes TNF-α-induced cell death via NF-κB and MAPK. In our study, DPI, a NADPH inhibitor, and NAC, a ROS scavenger, inhibited TNF-α-induced activation of Mst1 and caspase 3 as well as apoptosis of ECs. These data suggest that ROS mediates TNF-α-induced Mst1 activation and apoptosis. The direct activation of Mst1 by H_2O_2 in VSMCs may support this idea [24]. A recent study identified FOXO 3, a transcription factor inducing apoptosis or adaptive responses upon exposure to oxidative stress, as a target molecule of Mst1 [29]. Activation of Mst1 by H_2O_2 induced phosphorylation of FOXO 3 at serine 207, which is distinct from the phosphorylation site by Akt and disrupts the interaction with 14-3-3 proteins. The dissociation from 14-3-3 proteins promotes FOXO 3 nuclear translocation and induces cell death in neurons. It is not clear whether the same pathway is involved in TNF-α-induced apoptosis of EC, because the antibody that recognizes phosphorylated FOXO 3 at serine 207 is not available. However, it is possible that FOXO 3 is involved in TNF-α-induced EC apoptosis in the downstream of Mst1.

DPI is generally believed to inhibit NADPH oxidase. TNF-α receptor-associated factors (TRAFs) serve as scaffold protein that link ligand-occupied receptors of the TNF superfamily to other signaling molecules such as NF-κB and MAPK, and play important roles in TNF-α

signal cascade. Li et al. [30] reported that TNF-α induced rapid phosphorylation of $p47^{phox}$, a subunit of EC NADPH oxidase complex, resulting in the $p47^{phox}$-TRAF4 association and ROS production. Li et al. [31], however, reported that DPI inhibited mitochondrial superoxide production in monocytes. The author suggests that DPI inhibits mitochondrial NADP ubiquinone oxidoreductase. It is not clear whether the ROS induced by TNF-α are derived from NADPH oxidase or mitochondria at this point.

It has been reported that activated Mst1 induces caspase 3 activation, suggesting a positive feedback loop between Mst1 and caspase 3 [22]. However, we showed that knockdown of Mst1 by siRNA did not affect TNF-α-induced caspase 3 activation. Because Z-DEVD-FMK, a caspase 3 inhibitor, inhibited TNF-α-induced Mst1 activation, Mst1 is a downstream molecule of caspase 3. Therefore, the positive feedback loop between Mst1 and caspase 3 is not formed in the TNF-α-signaling pathway. Knockdown of Mst1 attenuated, but not completely inhibited, TNF-α-induced EC apoptosis. Therefore, it is suggested that Mst1-dependent and independent pathways are involved in TNF-α-induced apoptosis.

Developing plaques are reported to be associated with increased EC turnover rate possibly due to an increase in apoptosis [32]. It is also reported that regenerated EC is dysfunctional [33] and therefore atherogenic rather than antiatherogenic. We previously reported that vascular injury upregulated and activated Mst1 in rat carotid artery [24]. Therefore, Mst1 may enhance apoptosis of ECs, which may result in the progression of atherosclerosis. In addition, EC apoptosis induces an exposure of phosphatidylserine to the vessel lumen, which enhances tissue factor activity resulting in an increase in thrombogenicity and may induce acute coronary syndrome.

In conclusion, we showed compelling evidence that Mst1 is involved in TNF-α-induced EC apoptosis in the present study. Mst1 may be a therapeutic target for inhibiting EC apoptosis and maintaining EC integrity to prevent progression and unstabilization of atherosclerotic plaque.

Acknowledgments

This study was supported in part by a Grants-in-Aid for Scientific Research from ministry of Education, Culture, Sports, Science and Technology of Japan (17590742) to T.I.

Appendix A. Supplementary data

Supplementary data associated with this article can be found, in the online version, at doi:10.1016/j.bbrc.2007.12.173.

References

[1] M. Valgimigli, E. Merli, P. Malagutti, O. Soukhomovskaia, G. Cicchitelli, G. Macri, R. Ferrari, Endothelial dysfunction in acute and chronic coronary syndromes: evidence for a pathogenetic role of oxidative stress, Arch. Biochem. Biophys. 420 (2003) 255–261.

[2] A. Warnholtz, G. Nickenig, E. Schulz, R. Macharzina, J.H. Brasen, M. Skatchkov, T. Heitzer, J.P. Stasch, K.K. Griendling, D.G. Harrison, M. Bohm, T. Meinertz, T. Munzel, Increased NADH-oxidase-mediated superoxide production in the early stages of atherosclerosis: evidence for involvement of the renin-angiotensin system, Circulation 99 (1999) 2027–2033.

[3] J. Plutzky, Inflammatory pathways in atherosclerosis and acute coronary syndromes, Am. J. Cardiol. 88 (2001) 10K–15K.

[4] R. Ross, Atherosclerosis—an inflammatory disease, N. Engl. J. Med. 340 (1999) 115–126.

[5] G.K. Hansson, Immune mechanisms in atherosclerosis, Arterioscler. Thromb. Vasc. Biol. 21 (2001) 1876–1890.

[6] P. Barath, M.C. Fishbein, J. Cao, J. Berenson, R.H. Helfan, J.S. Forrester, Detection and localization of tumor necrosis factor in human atheroma, Am. J. Cardiol. 65 (1990) 297–302.

[7] G. Haraldsen, D. Kvale, B. Lien, I.N. Farstad, P. Brandtzaeg, Cytokine-regulated expression of E-selectin, intercellular adhesion molecule-1 (ICAM-1), and vascular cell adhesion molecule-1 (VCAM-1) in human microvascular endothelial cells, J. Immunol. 156 (1996) 2558–2565.

[8] A. Cho, J. Graves, M.A. Reidy, Mitogen-activated protein kinases mediate matrix metalloproteinase-9 expression in vascular smooth muscle cells, Arterioscler. Thromb. Vasc. Biol. 20 (2000) 2527–2532.

[9] I.M. Loftus, A.R. Naylor, S. Goodall, M. Crowther, L. Jones, P.R. Bell, M.M. Thompson, Increased matrix metalloproteinase-9 activity in unstable carotid plaques. A potential role in acute plaque disruption, Stroke 31 (2000) 40–47.

[10] Z.S. Galis, G.K. Sukhova, M.W. Lark, P. Libby, Increased expression of matrix metalloproteinases and matrix degrading activity in vulnerable regions of human atherosclerotic plaques, J. Clin. Invest. 94 (1994) 2493–2503.

[11] B. Alvarez, C. Ruiz, P. Chacon, J. Alvarez-Sabin, M. Matas, Serum values of metalloproteinase-2 and metalloproteinase-9 as related to unstable plaque and inflammatory cells in patients with greater than 70% carotid artery stenosis, J. Vasc. Surg. 40 (2004) 469–475.

[12] E. Zouridakis, P. Avanzas, R. Arroyo-Espliguero, S. Fredericks, J.C. Kaski, Markers of inflammation and rapid coronary artery disease progression in patients with stable angina pectoris, Circulation 110 (2004) 1747–1753.

[13] P. Libby, P.M. Ridker, A. Maseri, Inflammation and atherosclerosis, Circulation 105 (2002) 1135–1143.

[14] P. Libby, G. Sukhova, R.T. Lee, Z.S. Galis, Cytokines regulate vascular functions related to stability of the atherosclerotic plaque, J. Cardiovasc. Pharmacol. 25 (1995) S9–S12.

[15] E. Durand, A. Scoazec, A. Lafont, J. Boddaert, A. Al Hajzen, F. Addad, M. Mirshahi, M. Desnos, A. Tedgui, Z. Mallat, In vivo induction of endothelial apoptosis leads to vessel thrombosis and endothelial denudation: a clue to the understanding of the mechanisms of thrombotic plaque erosion, Circulation 109 (2004) 2503–2506.

[16] T. Bombeli, B.R. Schwartz, J.M. Harlan, Endothelial cells undergoing apoptosis become proadhesive for nonactivated platelets, Blood 93 (1999) 3831–3838.

[17] S. Dimmeler, K. Breitschopf, J. Haendeler, A.M. Zeiher, Dephosphorylation targets Bcl-2 for ubiquitin-dependent degradation: a link between the apoptosome and the proteasome pathway, J. Exp. Med. 189 (1999) 1815–1822.

[18] F. Chen, P. Eriksson, T. Kimura, I. Herzfeld, G. Valen, Apoptosis and angiogenesis are induced in the unstable coronary atherosclerotic plaque, Coron. Artery Dis. 16 (2005) 191–197.

[19] I. Dan, N.M. Watanabe, A. Kusumi, The Ste20 group kinases as regulators of MAP kinase cascades, Trends Cell Biol. 11 (2001) 220–230.

[20] K.K. Lee, T. Ohyama, N. Yajima, S. Tsubuki, S. Yonehara, MST, a physiological caspase substrate, highly sensitizes apoptosis both upstream and downstream of caspase activation, J. Biol. Chem. 276 (2001) 19276–19285.

[21] S. Yamamoto, G. Yang, D. Zablocki, J. Liu, C. Hong, S.J. Kim, S. Soler, M. Odashima, J. Thaisz, G. Yehia, C.A. Molina, A. Yatani, D.E. Vatner, S.F. Vatner, J. Sadoshima, Activation of Mst1 causes dilated cardiomyopathy by stimulating apoptosis without compensatory ventricular myocyte hypertrophy, J. Clin. Invest. 111 (2003) 1463–1474.

[22] J.D. Graves, Y. Gotoh, K.E. Draves, D. Ambrose, D.K. Han, M. Wright, J. Chernoff, E.A. Clark, E.G. Krebs, Caspase-mediated activation and induction of apoptosis by the mammalian Ste20-like kinase Mst1, EMBO J. 17 (1998) 2224–2234.

[23] S. Ura, N. Masuyama, J.D. Graves, Y. Gotoh, MST1-JNK promotes apoptosis via caspase-dependent and independent pathways, Genes Cells 6 (2001) 519–530.

[24] H. Ono, T. Ichiki, H. Ohtsubo, K. Fukuyama, I. Imayama, Y. Hashiguchi, J. Sadoshima, K. Sunagawa, Critical role of Mst1 in vascular remodeling after injury, Arterioscler. Thromb. Vasc. Biol. 25 (2005) 1871–1876.

[25] T. Tokunou, T. Ichiki, K. Takeda, Y. Funakoshi, N. Iino, H. Shimokawa, K. Egashira, A. Takeshita, Thrombin induces interleukin-6 expression through the cAMP response element in vascular smooth muscle cells, Arterioscler. Thromb. Vasc. Biol. 21 (2001) 1759–1763.

[26] C. Fleury, B. Mignotte, J.L. Vayssiere, Mitochondrial reactive oxygen species in cell death signaling, Biochimie 84 (2002) 131–141.

[27] M. Aoki, T. Nata, R. Morishita, H. Matsushita, H. Nakagami, K. Yamamoto, K. Yamazaki, M. Nakabayashi, T. Ogihara, Y. Kaneda, Endothelial apoptosis induced by oxidative stress through activation of NF-kappaB: antiapoptotic effect of antioxidant agents on endothelial cells, Hypertension 38 (2001) 48–55.

[28] H. Kamata, S. Honda, S. Maeda, L. Chang, H. Hirata, M. Karin, Reactive oxygen species promote TNFalpha-induced death and sustained JNK activation by inhibiting MAP kinase phosphatases, Cell 120 (2005) 649–661.

[29] M.K. Lehtinen, Z. Yuan, P.R. Boag, Y. Yang, J. Villen, E.B. Becker, S. DiBacco, N. de la Iglesia, S. Gygi, T.K. Blackwell, A. Bonni, A conserved MST-FOXO signaling pathway mediates oxidative-stress responses and extends life span, Cell 125 (2006) 987–1001.

[30] J.M. Li, L.M. Fan, M.R. Christie, A.M. Shah, Acute tumor necrosis factor alpha signaling via NADPH oxidase in microvascular endothelial cells: role of p47phox phosphorylation and binding to TRAF4, Mol. Cell Biol. 25 (2005) 2320–2330.

[31] Y. Li, M.A. Trush, Diphenyleneiodonium, an NAD(P)H oxidase inhibitor, also potently inhibits mitochondrial reactive oxygen species production, Biochem. Biophys. Res. Commun. 253 (1998) 295–299.

[32] S. Dimmeler, C. Hermann, A.M. Zeiher, Apoptosis of endothelial cells. Contribution to the pathophysiology of atherosclerosis? Eur. Cytokine Netw. 9 (1998) 697–698.

[33] M.P. Fournet-Bourguignon, M. Castedo-Delrieu, J.P. Bidouard, S. Leonce, D. Saboureau, I. Delescluse, J.P. Vilaine, P.M. Vanhoutte, Phenotypic and functional changes in regenerated porcine coronary endothelial cells: increased uptake of modified LDL and reduced production of NO, Circ. Res. 86 (2000) 854–861.

Cardiovascular Research (2008) 77, 713–721
doi:10.1093/cvr/cvm092

Modulation of the myocardial redox state by vagal nerve stimulation after experimental myocardial infarction

Takaki Tsutsumi[1], Tomomi Ide[1]*, Mayumi Yamato[2], Wataru Kudou[2], Makoto Andou[1], Yoshitaka Hirooka[1], Hideo Utsumi[3], Hiroyuki Tsutsui[4], and Kenji Sunagawa[1]

[1]*Department of Cardiovascular Medicine, Graduate School of Medical Sciences, Kyushu University, 3-1-1 Maidashi, Higashi-ku, Fukuoka 812-8582, Japan;* [2]*Department of REDOX Medicinal Science, Graduate School of Pharmaceutical Sciences, Kyushu University, Fukuoka, Japan;* [3]*Laboratory of Bio-function Analysis, Graduate School of Pharmaceutical Sciences, Kyushu University, Fukuoka, Japan; and* [4]*Cardiovascular Medicine, Hokkaido University Graduate School of Medicine, Sapporo, Japan*

Received 16 July 2007; revised 24 November 2007; accepted 30 November 2007; online publish-ahead-of-print 7 December 2007

Time for primary review: 13 days

KEYWORDS
Autonomic nervous system;
Acetylcholine;
Heart failure;
Oxidative stress

Aims Redox alteration plays a major role in the pathogenesis of heart failure (HF). Since vagal nerve stimulation (VNS) is known to improve survival and attenuate cardiac remodelling, we hypothesized that VNS may modulate the myocardial redox state.

Methods and results Using a chronic HF mouse model, we applied VNS for 15 min and measured myocardial redox status using *in vivo* electron spin resonance spectroscopy. Signal decay rate of the nitroxyl probe, an index of redox status, was enhanced in HF compared with sham (0.16 ± 0.01 vs. $0.13 \pm 0.01\ min^{-1}$, $P < 0.05$; $n = 6$), and VNS normalized this enhancement ($0.13 \pm 0.01\ min^{-1}$, $P < 0.05$). Atropine sulphate abolished the VNS effects, indicating that the VNS modulates myocardial redox state via muscarinic receptors. N_{ω}-Nitro-L-arginine methyl ester treatment and fixed-rate atrial pacing showed a trend to suppress the VNS effects, suggesting the involvement of nitric oxide-based signalling and myocardial oxygen consumption. Moreover, VNS decreased the myocardial norepinephrine (NE) level (0.25 ± 0.07 vs. 0.60 ± 0.12 ng/mL, $P < 0.05$; $n = 6$). Reactive oxygen species production from cultured cardiomyocytes was enhanced by β-adrenergic activation, which was partially antagonized by 10 μmol/L acetylcholine (ACh) (relative value compared with control: NE 3.7 ± 0.5, NE + ACh 2.5 ± 0.3, $P < 0.05$; $n = 12$).

Conclusion The present study suggests that VNS modulates the cardiac redox status and adrenergic drive, and thereby suppresses free radical generation in the failing heart.

1. Introduction

Accumulating evidence has revealed an intimate link between the imbalance of autonomic nervous system and the pathogenesis of chronic heart failure (CHF).[1] Suppressed vagal tone and over-activated sympathetic drive accelerate cardiac remodelling and increase the risk of life-threatening tachyarrhythmia.[2] Although beta-blocker therapy aiming to antagonize the adrenergic drive is a standard treatment for CHF, the prognosis remains poor.[3]

Extensive studies and evidence have demonstrated an excessive generation of reactive oxygen species (ROS) in the failing hearts.[4–6] ROS are implicated in several pathways in CHF, such as the rennin–angiotensin–aldosterone system[7] and beta-adrenergic pathways.[8] ROS have also been proposed to alter gene expression, induce Ca^{2+} overload,[9] and activate apoptosis cascades in cardiomyocytes.[10] Furthermore, we have reported that reducing ROS by overexpressing antioxidant enzymes attenuates cardiac remodelling.[11]

Recently, Li *et al.*[12] have demonstrated that electrical stimulation of vagal nerve in post-myocardial infarction (MI)-induced CHF rats attenuates cardiac remodelling and markedly improves the prognosis, suggesting that active correction of the autonomic nervous imbalance may be a new therapeutic strategy. However, the precise mechanisms of the anti-remodelling effect of vagal nerve stimulation (VNS) have not been elucidated. It is well known that vagal nerve suppresses not only the cardiac function[13] but also cardiac sympathetic activity.[14] Moreover, electrical stimulation of cardiac parasympathetic nerve was reported to attenuate norepinephrine (NE) spillover in the left ventricle (LV), especially in the CHF animal.[15,16]

In this study, therefore, we proposed the following hypotheses: first, VNS attenuates the generation of ROS in

* Corresponding author. Tel: +81 92 642 5360; fax: +81 92 642 5374.
E-mail address: tomomi_i @cardiol.med.kyushu-u.ac.jp

the failing hearts. Secondly, redox regulation is mediated by both a decrease of cardiac NE spillover through attenuation of the cardiac sympathetic drives and a direct effect of acetylcholine (ACh) on the LV. Thirdly, NADPH oxidase is involved in the redox modulation by VNS. We tested these hypotheses *in vivo* using a murine model of CHF and *in vitro* using cultured neonatal rat cardiomyocytes.

Conventionally, it has been difficult to determine the free radical reactions or redox status *in vivo*, because free radicals and oxidants are unstable and highly reactive. The development of low frequency electron spin resonance (ESR) spectroscopy has allowed direct detection of free radicals[17] and direct estimation of the redox status in living animals non-invasively.[18] The advent of this technique has permitted the assessment of the contribution of free radicals in various pathological conditions.[19] In this study, we used *in vivo* ESR spectroscopy to evaluate a cardiac redox alteration following VNS.

We herein demonstrated for the first time that short VNS modulates the cardiac redox status and adrenergic drive, and thereby suppresses free radical generation in the failing heart.

2. Methods

2.1 Animal model of heart failure

All procedures and animal care were approved by the Committee on Ethics of Animal Experiment, Kyushu University Graduate School of Medical and Pharmaceutical Sciences and performed in accordance with the Guideline for Animal Experiment of Kyushu University, and the *Guide for the Care and Use of Laboratory Animals* published by the US National Institutes of Health (NIH Publication No. 85-23, revised 1996).

We used a murine model of CHF 28 days after induction of MI. The surgical procedure was described previously.[11] Briefly, 8–10 week-old male CD-1 mice weighing 30–35 g were used. Under anaesthesia with pentobarbital sodium (30 μg/g BW, i.p.), experimental MI was induced by ligating the left coronary artery. Control mice received sham operation without coronary artery ligation. Mice were housed in a temperature- and humidity-controlled room and fed a commercial diet and provided water *ad libitum*.

2.2 Echocardiographic and haemodynamic measurements

CHF ($n = 12$) and sham mice ($n = 12$) underwent physiological evaluation by echocardiography and left heart catheterization as previously reported.[11] Under light anaesthesia with tribromoethanol-amylene hydrate (2% Avertin, 8 μL/g BW, i.p.), two-dimensional targeted M-mode images were obtained from the short-axis view at the level of greatest LV dimension using a 7.5-MHz transducer connected to a dedicated ultrasonographic system (SSD-5500, ALOKA Co. Ltd., Tokyo, Japan). After echocardiography, a 1.4-F micromanometer-tipped catheter (Millar Instruments, Inc. Houston, TX, USA) was inserted into the right carotid artery and advanced into the LV for pressure measurement. Thereafter, mice were euthanized with overdose pentobarbital sodium. Heart and lungs were quickly excised and weighed.

2.3 Vagal nerve stimulation

CHF or control mice were randomly assigned to VNS ($n = 6$) and sham-stimulation (SS) group ($n = 6$). Under anaesthesia with pentobarbital sodium (30 μg/g BW, i.p.), the right vagal nerve was attached with a pair of stainless wire electrodes (Bioflex wire AS633; Cooner wire, Chatsworth, CA, USA) and covered with silicone

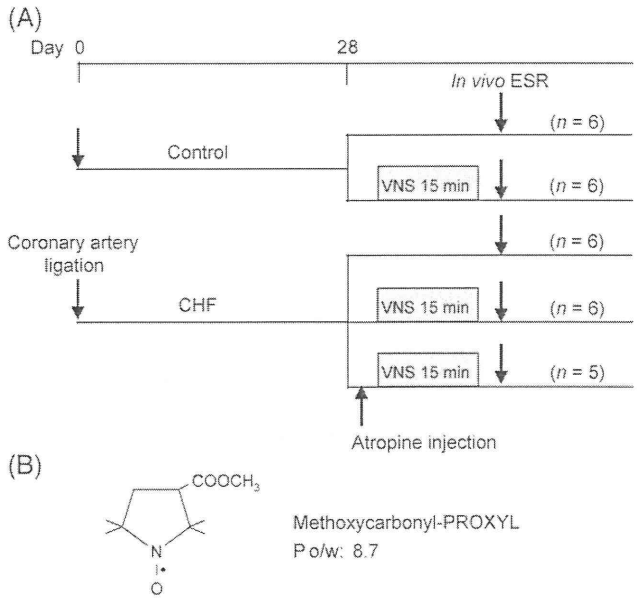

Figure 1 (*A*) Protocol scheme of the *in vivo* study in mice. Mice that survived 28 days after experimental myocardial infarction were used as a model of chronic heart failure (CHF). In CHF and sham operated control mice, sham or vagal nerve stimulation was conducted. After stimulation, methoxycarbonyl-PROXYL was injected and thereafter *in vivo* electron spin resonance (ESR) spectroscopy was performed. (*B*) Structure of methoxycarbonyl-PROXYL, a lipophilic nitroxide probe (oil : water ratio = 8.7).

gel for insulation and immobilization. The vagal nerve was stimulated with 10 Hz rectangular pulses of 1 ms duration for 15 min. Electrical voltage was optimized for each mouse so that the heart rate (HR) was reduced by 10% from baseline. In SS group, wire electrodes were implanted but VNS was not applied. Five minutes after VNS, mice subsequently underwent *in vivo* ESR analysis as described below. In a separate series of experiments, CHF mice were given intravenous injection of atropine sulphate (1 μg/g BW, Sigma-Aldrich, Inc., St Louis, MO, USA), followed by VNS, rectangular pulses of which were 10 Hz, and duration is 1 ms (*Figure 1A*). Electrical voltage was fixed at 500 mV, because muscarinic blockade abolishes the VNS induced HR reduction, and this electrical condition could reduce HR in almost all CHF and control mice.

In another series of experiments, we performed fixed rate atrial pacing during VNS to determine the impact of bradycardia. In brief, after implantation of electrical wires, the left chest was opened under artificial ventilation. A pair of stainless wires was surgically attached with left atrium. After HR reached constant, VNS and fixed rate atrial pacing were simultaneously initiated. The vagal nerve was stimulated with rectangular pulses of 1-ms duration, 10 Hz, 500 mV for 15 min. Rectangular pulses for atrial pacing were also of 1-ms duration. After 15 min of VNS and atrial pacing, the chest was closed and mice subsequently underwent *in vivo* ESR.

To elucidate the role of nitric oxide (NO) pathway, we applied VNS in mice treated with N_{ω}-nitro-L-arginine methyl ester (L-NAME) hydrochloride (Sigma-Aldrich). L-NAME (1 mg/kg/day) was administered to CHF mice through drinking water for 7 days prior to the experiment. The condition of VNS was same as in CHF + VNS mice.

2.4 *In vivo* electron spin resonance spectroscopy

We performed *in vivo* ESR spectroscopy to assess the myocardial redox state. This method is based on the theory that nitroxyl radicals are reduced to the corresponding hydroxylamine in the presence of free radicals *in vivo*, resulting in the disappearance of ESR signals.[18] A semilogarithmic plot of time course of the ESR signals shows a linear decay curve, the rate of which (a reciprocal

number of time constant) is proportional to the amount of reductants including free radicals. Prior to *in vivo* ESR analysis, mice were given intravenous injection of 3-methoxycarbonyl-2,2,5,5,5-tetramethylpyrrolidine-l-oxyl (methoxycarbonyl-PROXYL) (0.3 μmol/L/g BW), a membrane permeable nitroxyl spin probe (oil : water ratio = 8.7) (*Figure 1B*), which was synthesized as described previously.[20] Shortly thereafter, ESR spectra were recorded at regular intervals at chest region using L-band ESR spectrometer (JEOL Co. Ltd., Akishima, Japan) with a loop-gap resonator (33 mm i.d. and 30 mm in length). The power of the 1.1 GHz microwave was 1.67 mW.

First, as a validation study, we performed *in vivo* ESR in control and CHF mice, to which VNS were not applied, to determine whether the difference in signal decay could be observed between these mice. Secondly, we assessed the effect of two ROS scavengers, 1,2-dihydroxy-3,5-benzenedisulphonic acid disodium salt monohydrate (tiron) (10 μmol/mouse, Dojindo Molecular Lanoratories Co. Ltd., Kumamoto, Japan) and dimethylthiourea (DMTU) (10 μmol/mouse, Sigma-Aldrich), on ESR signal decay. These chemicals were administered intravenously prior to methoxycarbonyl-PROXYL injection. Thirdly, we performed *in vivo* ESR in CHF and control mice after VNS or SS.

2.5 Cardiac level of low molecular weight thiols

Cardiac level of low molecular weight thiols, which is mainly reduced glutathione (GSH), was measured by the 5,5′-dithiobis(2-nitrobenzoic acid) (DTNB) method. After sham or vagal stimulation for 15 min ($n = 6$ each), CHF mice were euthanized and hearts were quickly excised. Non-infarcted LV was homogenized with 4% sulphosalicylic acid and 10 μL of supernatant was incubated with 125 μL of 1.5 mmol/L DTNB at 37°C for 15 min. Absorbance at 405 nm was measured. Thiol concentration was determined by calibration using 0–2 mmol/L GSH, and was expressed as μmol/L/mg tissue.

2.6 Cytochrome *c* reduction assay

NADPH oxidase activity was examined using superoxide dismutase inhibitable cytochrome *c* reduction assay. After sham or vagal stimulation for 15 min, mice were euthanized and the heart was quickly excised. Non-infarcted LV sample was immediately homogenized with phosphate buffer saline. Ten μL of the supernatants (final concentration 3 mg/mL) were diluted in 190 μL of assay buffer (300 mmol/L potassium phosphate, 0.1 mmol/L EDTA, 36 μmol/L cytochrome *c*, pH 7.8) in 96-well plates. NADPH (1 μmol/L) was added in the presence or absence of SOD (200 U/mL). Cytochrome *c* reduction was measured by reading the absorbance at 550 nm on microplate reader. NADPH oxidase activity was calculated from the difference between the absorbance with or without SOD and the extinction coefficient (21.1 mmol/L/cm) for reduced cytochrome *c*. Cytochrome *c* reductase positive control (Sigma-Aldrich) was used to verify the specificity of the assay. Results were expressed as unit/mL, which was defined as reduction in 1.0 μmol of oxidized cytochrome *c* in the presence of 100 μmol/L NADPH per minute at pH 7.8 at 25°C.

2.7 Cardiac level of norepinephrine

Cardiac level of NE was measured by microdialysis and high performance liquid chromatography (HPLC). We used a transverse dialysis probe consisted of a dialysis fibre (2 mm in length, 220 μm in outer diameter, 200 μm in inner diameter, molecular weight cutoff at 50 kDa; OP-50-2, Eikom, Kyoto, Japan). Under light anaesthesia with pentobarbital sodium (20 μg/g BW, i.p.), mice were mechanically ventilated. After implantation of electrical wires, the left chest was opened. A dialysis probe was implanted into the non-infarcted LV. Ringer's solution (Na^+; 147 mmol/L, K^+; 4 mmol/L, Ca^{2+}; 1.26 mmol/L, Mg^{2+}; 1 mmol/L, Cl^-; 155.6 mmol/L) was pumped at a constant flow rate of 2 μL/min. Microdialysis session was started after a 30-min equilibration period. After collecting pre-VNS (baseline) samples for 30 min, VNS was started. From 15 min after VNS initiation, VNS samples were collected for 30 min. Finally, post-VNS samples were collected 15 min after the termination of VNS. NE concentration was assayed by HPLC, the condition of which was described in Supplementary Method.

2.8 Reactive oxygen species production in cultured neonatal rat ventricular cardiomyocytes

Primary cultures of cardiomyocytes were prepared from the ventricles of neonatal Wistar rats as described previously.[21] Briefly, after digestion of the myocardial tissue with trypsin, cells were suspended in Dulbecco's Modified Eagle's Medium (Sigma-Aldrich) containing 10% FBS and preplated twice in 100-mm culture dishes for 70 min each to reduce the number of non-myocytes. Non-adherent cells were plated in 12-well cultured plates at a density of 10^3 cells per mm^2. Cardiomyocytes were maintained at 37°C in humidified air with 5% CO_2. The culture medium was replaced by Hanks' balanced salt solution with Ca^{2+} and Mg^{2+} but without phenol red (Gibco, Invitrogen, Carlsbad, CA, USA) 24 h before the experiments.

On culture day 4, cells were exposed to NE (Sigma-Aldrich) in concentration from 0.01 to 100 μmol/L under the simultaneous incubation with prazosin hydrochloride (0.1 μmol/L) (Sigma-Aldrich) for 30 min to determine the ROS production from cardiomyocytes in response to β-adrenergic activation. H_2O_2 concentration in the culture medium was measured as described below. In a separate series of experiments, to elucidate the effect of ACh on the ROS production via β-adrenergic activation, cells were incubated with NE (10 μmol/L), NE + ACh (10 μmol/L) (Sigma-Aldrich), and NE + ACh + atropine hydrochloride (10 μmol/L) (Sigma-Aldrich). All NE-treated cells were incubated with 0.1 μmol/L prazosin. ACh and atropine were added 30 min prior to NE exposure. In the experiment to elucidate the ROS production within the myocytes, cells were incubated with 5 μmol/L of 2′,7′-dichlorofluorescin diacetate (DCFH-DA) (Sigma-Aldrich) at 37°C for 30 min. The fluorescence images were acquired with a microscope (BX50, Olympus Co. Ltd., Tokyo, Japan). Relative intensity for treated cells was determined by comparing with control cells. The experiment was repeated three times independently. For an experiment to determine the extracellular ROS production, after incubation at 37°C for 30 min, we collected the conditioned culture medium.

The H_2O_2 concentration was measured by the method reported by Keston and Brandt.[22] In brief, 10 μL of sample ($n = 10$ each) was reacted *in vitro* with 1 μmol/L DCFH-DA. Oxidation of DCFH-DA to the fluorescent 2-7-dichlorofluorescein (DCF) by H_2O_2 was investigated by measuring fluorescence at an excitation wavelength of 510 nm and an emission wavelength of 550 nm. The fluorescence intensity was corrected by subtracting the value of the sample treated with catalase. The concentration of H_2O_2 was determined by calibration using 0–10 μmol/L H_2O_2.

2.9 Statistical analysis

Data are presented as mean ± SEM. Significant differences were determined by one-way analysis of variance using the Tukey post hoc test. Myocardial NE concentrations before and during VNS were compared by a paired *t*-test, after confirming normal distribution. A *P*-value less than 0.05 was judged to represent a statistically significant difference.

3. Results

3.1 Animal characteristics

LV dimensions were significantly enlarged and systolic function was significantly reduced in CHF, compared with control mice (*Table 1*). Although there was no significant difference in HR, the values of mean aortic pressure, LV + d*p*/d*t* max

and $-dp/dt$ max were lower, and LV end-diastolic pressure was higher in CHF than in control. Heart weight/body weight, LV weight/body weight, and lung weight have also increased in CHF. Four mice out of 12 had obvious pleural effusion, whereas no effusion was present in control mice.

Table 1 *Characteristics of the chronic heart failure (CHF) mouse model*

	Control ($n = 12$)	CHF ($n = 12$)
Body weight (g)	40.0 ± 0.5	39.1 ± 0.8
Echocardiographic data		
Heart rate (bpm)	539 ± 13	535 ± 27
LVEDD (mm)	3.6 ± 0.1	5.9 ± 0.2*
LVESD (mm)	2.1 ± 0.3	5.5 ± 0.3*
FS (%)	42.9 ± 1.0	6.8 ± 0.9*
Haemodynamic data		
Mean AoP (mmHg)	89 ± 3	76 ± 4*
LVEDP (mmHg)	2.5 ± 0.2	16.6 ± 1.7*
+ dp/dt max (mmHg/s)	12900 ± 400	4900 ± 400*
− dp/dt max (mmHg/s)	−8600 ± 300	−3300 ± 200*
Organ weight data		
Heart wt/body wt (mg/g)	4.9 ± 0.1	10.8 ± 0.3*
LV wt/body wt (mg/g)	3.0 ± 0.1	4.0 ± 0.1*
Lung weight (mg)	183 ± 4	366 ± 20*

LV, left ventricular; EDD, end-diastolic diameter; ESD, end-systolic diameter; FS, fractional shortening; AoP, aortic pressure; EDP, end-diastolic pressure; wt, weight. Values are mean ± SEM.
$P < 0.05$ and *$P < 0.01$ vs. control.

3.2 Measurement of reactive oxygen species by *in vivo* electron spin resonance

The signal decay rate of methoxycarbonyl-PROXYL at the chest region in CHF mice was clearly enhanced compared with controls (*Figure 2A*). This increased signal decay rate was almost reversed by the treatment with tiron or DMTU (*Figure 2B*), suggesting that the total redox state was changed probably due to increased ROS production especially in the failing myocardium.

In the next VNS protocol, VNS elicited a similar HR reduction in both CHF and control mice. Although there were some minor differences in each animal, from 300 to 500 mV were needed to reduce HR by 10% from baseline. No HR reduction by electrical stimulation (500 mV) was observed in CHF mice treated with atropine. *In vivo* ESR spectroscopy revealed that VNS normalized the enhanced signal decay in CHF mice. In control mice, VNS showed no effects on the signal decay rate. Furthermore, this vagal-mediated effect in CHF mice was abolished by the administration of atropine (*Figure 2C*). These results suggested that VNS normalized the altered redox state in the failing myocardium potentially through attenuating the overproduction of ROS via muscarinic ACh receptor pathway.

As an additional series of experiments, we performed *in vivo* ESR in CHF mice under fixed rate atrial pacing to exclude the effects of bradycardia. Fixed rate pacing showed a trend to abolish the VNS effects (*Figure 3A*).

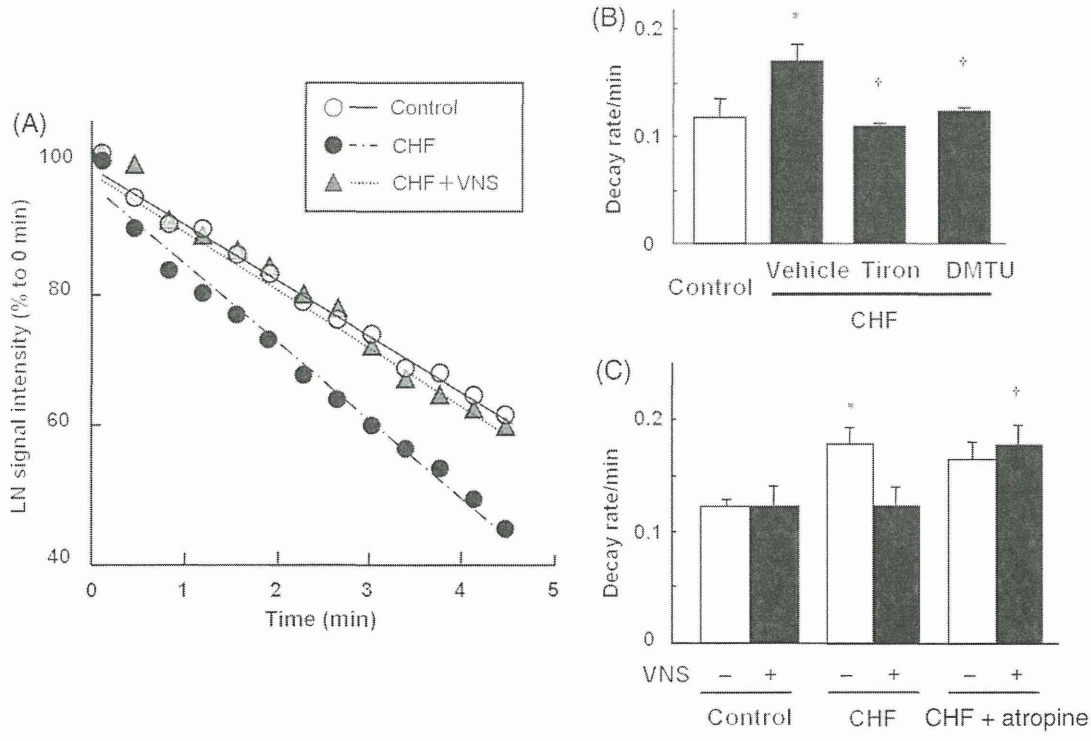

Figure 2 Effects of vagal nerve stimulation (VNS) on the signal decay of methoxycarbonyl-PROXYL at the chest region in control and chronic heart failure (CHF) mice with or without VNS. The electron spin resonance (ESR) signal decay curve was obtained by plotting the peak height of the ESR signals semilogarithmically as a function of time. (*A*) Typical *in vivo* ESR signal decay curves of methoxycarbonyl-PROXYL in control mouse (○), CHF mouse without VNS (●) and CHF mouse with VNS (?). Solid and broken lines are linear fits to the respective data. (*B*) Signal decay rates (calculated from the slopes of fitted lines) in CHF mice administered vehicle or the antioxidant tiron (400 μmol/kg) or DMTU (400 μmol/kg). *$P < 0.05$ vs. control; †$P < 0.05$ vs. CHF-vehicle, $n = 6$ in each group. (*C*) Signal decay rates in mice of control, CHF and CHF with atropine administration. *$P < 0.05$ vs. control without VNS; †$P < 0.05$ vs. CHF with VNS, $n = 5$ in CHF with atropine administration group, $n = 6$ in other groups. The data in B and C are presented as means ± SEM.

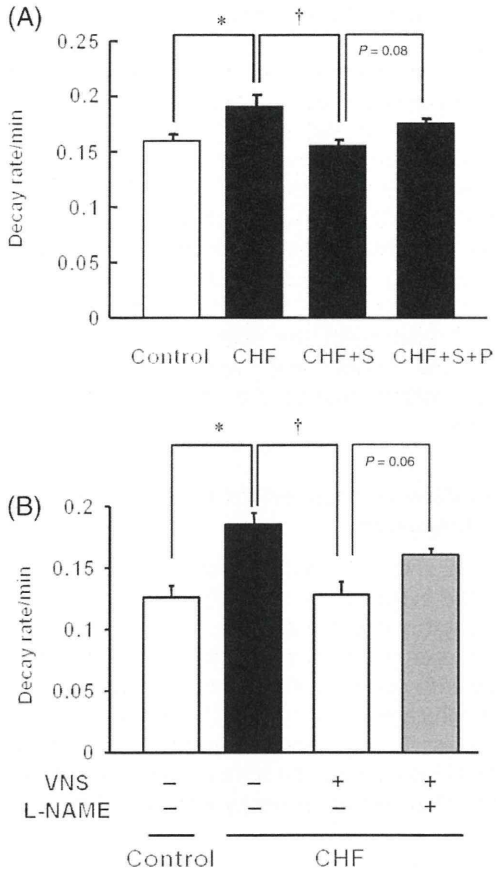

Figure 3 (*A*) *In vivo* electron spin resonance signal decay rates in mice of control, chronic heart failure (CHF), CHF + vagal nerve stimulation (VNS) (CHF + S), and CHF + VNS under fixed rate pacing (CHF + S + P). $^{*}P < 0.05$ vs. control; $^{\dagger}P < 0.05$ vs. CHF, *P*-value between CHF + S and CHF + S + P was 0.08. $n = 7$ in group of control and CHF, $n = 5$ in group of CHF + S and CHF + S + P. (*B*) Signal decay rates in mice of control, CHF, CHF + VNS, and CHF + VNS with N_{ω}-nitro-L-arginine methyl ester (L-NAME) (1 mg/kg/day). L-NAME treatment showed a tendency for attenuating the VNS induced antioxidative effects ($P = 0.062$ vs. CHF + VNS). $^{*}P < 0.05$ vs. control; $^{\dagger}P < 0.05$ vs. CHF, $n = 7$ in group of control and CHF, $n = 6$ in group of CHF + VNS and CHF + VNS + L-NAME. The data are presented as means ± SEM.

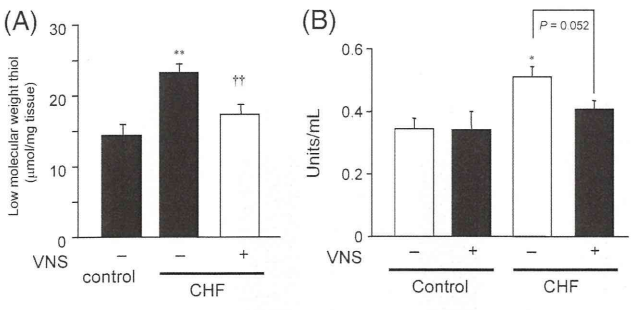

Figure 4 (*A*) Effects of vagal nerve stimulation (VNS) on cardiac concentration of low molecular thiols. The values are means ± SEM, $n = 6$ in each group. $^{**}P < 0.01$ vs. control without VNS; $^{\dagger\dagger}P < 0.01$ vs. chronic heart failure (CHF) without VNS. (*B*) Myocardial NADPH oxidase activity. $^{*}P < 0.05$ vs. control without VNS. $n = 6$ in each group.

Furthermore, we also performed *in vivo* ESR analysis in CHF mice treated with L-NAME to clarify the involvement of NO. L-NAME treated mice showed a diminished HR response to VNS and a tendency to reduce the VNS induced improvements in myocardial redox state (*Figure 3B*).

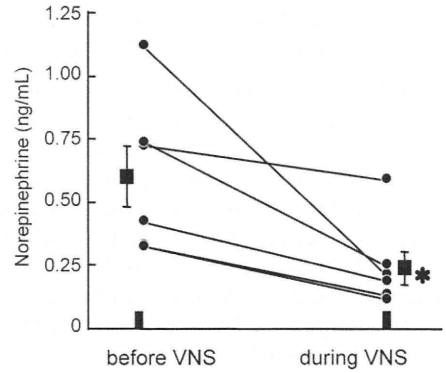

Figure 5 Cardiac norepinephrine levels with or without vagal nerve stimulation (VNS), assessed by microdialysis and high performance liquid chromatography. Closed circles and lines indicate the level of norepinephrine before and during VNS in each animal. Squares and error bars indicate means ± SEM, $n = 6$ in each group. $^{*}P < 0.05$ vs. before VNS.

3.3 Cardiac concentration of low molecular weight thiols

The myocardial concentration of low molecular weight thiols was significantly increased in CHF compared with control mice, and the increase was significantly attenuated by 15-min VNS (*Figure 4A*). This result also supported the observation that the redox status in the failing myocardium was altered by short application of VNS.

3.4 Nicotinamide adenin dinucleotide phosphate (NADPH) oxidase activity

Western blot analysis and cytochrome *c* reduction assay were performed on LV samples taken from control or CHF mice after the VNS or SS. Although the myocardial expression of $p47^{phox}$, a cytosolic subunit of NADPH oxidase, was significantly increased in CHF mice, it was not altered after VNS (see Supplementary Methods and Supplementary material online, *Figure S1A and B*). Cytochrome *c* reduction assay revealed that myocardial NADPH oxidase activity was enhanced in CHF mice relative to control mice (0.51 ± 0.02 units/mL CHF + SS vs. 0.34 ± 0.03 units/mL control + SS, $P < 0.05$) and that there was a tendency for a reduction in NADPH oxidase acitivity by VNS (0.40 ± 0.03 units/mL CHF + VNS, $P = 0.052$) (*Figure 4B*).

3.5 Cardiac norepinephrine concentration

Cardiac NE concentration in CHF mice decreased significantly during VNS compared with before VNS (0.25 ± 0.07 ng/mL during VNS vs. 0.61 ± 0.12 ng/mL before VNS, $P < 0.05$) (*Figure 5*) and returned to baseline after the termination of VNS (0.43 ± 0.07 ng/mL after VNS vs. 0.25 ± 0.07 ng/mL during VNS, $P < 0.05$). Although it did not reach statistical significance, VNS induced reduction in NE level was also observed in control mice (0.47 ± 0.06 ng/mL before VNS, 0.36 ± 0.08 ng/mL during VNS, 0.42 ± 0.02 ng/mL after VNS, $P > 0.05$). These results suggested that VNS inhibited sympathetic nerve presynaptically especially in CHF mice.

3.6 β-Adrenergic receptor mediated reactive oxygen species production in cardiomyocytes

An increase in DCF fluorescence was observed 30 min after β-adrenergic receptor (β-AR) stimulation of cultured cardiomyocytes with 10 μmol/L NE. Furthermore, NE also increased the extracellular H_2O_2 release in a concentration-dependent manner (*Figure 6A*), confirming that β-AR stimulation increased the production of ROS in cardiomyocytes. The NE-induced DCFH oxidation was inhibited significantly by the addition of 10 μmol/L ACh, and this effect was abolished by atropine sulphate (*Figure 6B*), indicating that ACh directly inhibits the β-AR-stimulated ROS production in cardiomyocytes. The anti-oxidative effect of ACh was also demonstrated in NE-induced extracellular H_2O_2 release. ACh partially but significantly attenuated the NE-induced H_2O_2 release (46% reduction), which was also abolished by the addition of atropine sulphate (*Figure 6C*).

4. Discussion

The major findings demonstrated in the present study are that: (i) short VNS altered the myocardial redox status in CHF mice; (ii) this observation was mediated by both an inhibition of sympathetic drive and a direct action of ACh against free radical generation in the myocardium; and (iii) the subcellular mechanisms may involve NADPH oxidase activation, NO production, and myocardial oxygen consumption.

Cardiac parasympathetic nerve may play a defensive role in the pathogenesis of various heart diseases. According to the previous studies, VNS not only reduces the occurrence of lethal ventricular tachyarrhythmia[23,24] but also attenuates the development of cardiac remodelling.[12] In addition to these effects, the present study demonstrated that VNS suppresses myocardial ROS over-production. ROS cause cardiac apoptosis and activate several maladaptive cascades, which in turn lead to further dysfunction of cardiomyocytes.[10] Therefore, the vagal-mediated anti-oxidative effects in the failing heart may provide an important mechanism contributing to the anti-remodelling action of chronic VNS.

4.1 Alteration of myocardial redox state by vagal nerve stimulation

We used *in vivo* ESR spectroscopy with a spin probe to measure the excess amount of ROS generation or estimate the redox status in living animals.[18] CHF mice with marked LV systolic dysfunction showed enhanced ESR signal decay compared with controls. The increased signal decay rate in CHF mice indicates alteration of the redox status, probably due to excess ROS generation, because administration of antioxidants normalized the accelerated signal decay. Strikingly, the enhanced signal decay was almost normalized by

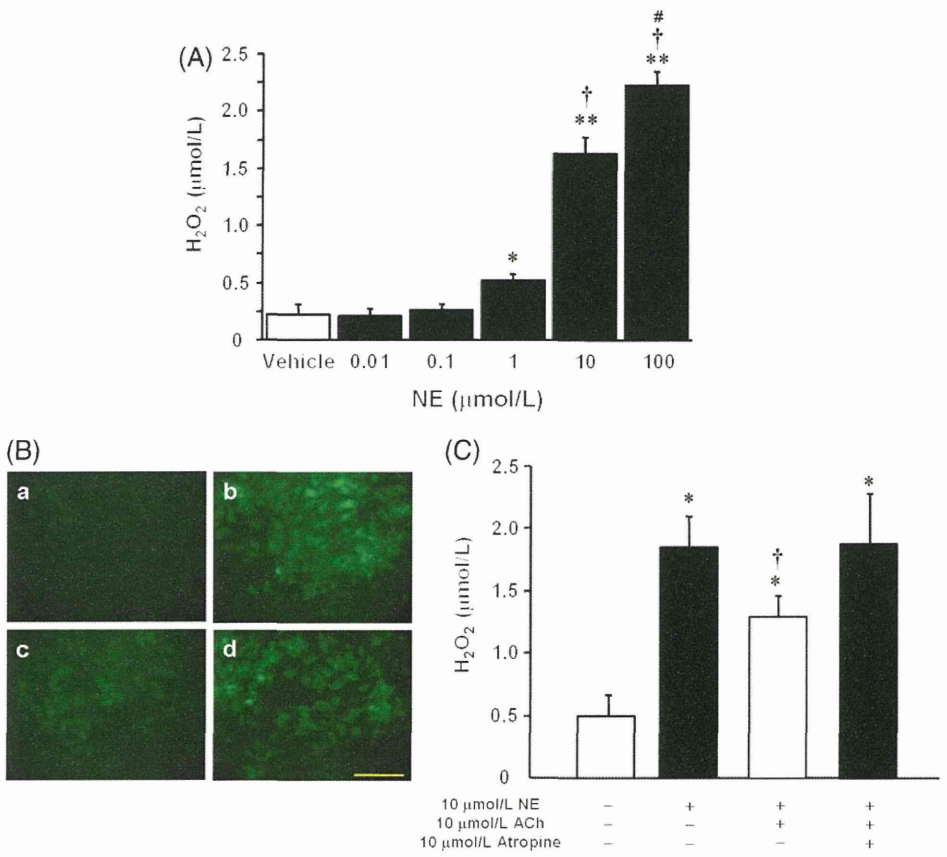

Figure 6 *In vitro* effects of acetylcholine (ACh) on norepinephrine (NE)-induced oxidants production in cardiomyocytes. (*A*) NE induced extracellular H_2O_2 release in a concentration-dependent manner. Values are means ± SEM, $n = 12$ in each group. $^*P < 0.05$ and $^{**}P < 0.01$ vs. vehicle; $^{\dagger}P < 0.05$ vs. 1 μmol/L NE; $^{\#}P < 0.05$ vs. 10 μmol/L NE. (*B*) Dichlorofluorescein fluorescence within cardiomyocytes. Cells were incubated with vehicle (a), 10 μmol/L NE (b), 10 μmol/L NE with 10 μmol/L ACh (c), 10 μmol/L NE with 10 μmol/L ACh in the presence of 10 μmol/L atropine (d). (*C*) Suppression of NE-induced extracellular H_2O_2 release by ACh. Values are means ± SEM, $n = 10$ in each group. $^*P < 0.05$ vs. vehicle; $^{\dagger}P < 0.05$ vs. 10 μmol/L NE.